Geomechanics and Engineering, *Vol. 16, No. 1 (2018) 59-69*
DOI: https://doi.org/10.12989/gae.2018.16.1.059

An improved radius-incremental-approach of stress and displacement for strain-softening surrounding rock considering hydraulic-mechanical coupling

Jin-Feng Zou* and Xing-Xing Wei

School of Civil Engineering, Central South University, No.22, Shaoshan South Road, Central South University Railway Campus, Changsha, Hunan Province, People's Republic of China, 410075

(Received April 13, 2017, Revised March 17, 2018, Accepted March 29, 2018)

Abstract. This study focused on the mechanical and hydraulic characteristics of underwater tunnels based on Mohr-Coulomb (M-C), Hoek-Brown (H-B) and generalized H-B failure criteria. An improved approach for calculating stress, displacement and plastic radius of the circular tunnel considering hydraulic-mechanical coupling was developed. The innovation of this study was that the radius-incremental-approach was reconstructed (i.e., the whole plastic zone is divided into a finite number of concentric annuli by radius), stress and displacement of each annulus were determined in terms of numerical method and Terzaghi's effective stress principle. The validation of the proposed approach was conducted by comparing with the results in Brown and Bray (1982) and Park and Kim (2006). In addition, the Rp-pin curve (plastic radius-internal supporting pressure curve) was obtained using the numerical iterative method, and the plastic radius of the deep-buried tunnel could be obtained by interpolation method in terms of the known value of internal supporting pressure pin. Combining with the theories in Carranza and Fairhurst (2000), the improved technique for assessing the reliability of the tunnel support was proposed.

Keywords: hydraulic-mechanical coupling; strain-softening; safety factor; finite difference method

1. Introduction

The constructions of tunnel and underground engineering have become more and more extensive. Many researchers have focused on this aspect and great contributions have made (e.g., Antonio 2016, Apostolos 2017, Boonchai *et al.* 2017, Do *et al.* 2014, Fahimifar and Zareifard 2014, Ieronymaki *et al.* 2017, Huang *et al.* 2017, Liu *et al.* 2017, Ochmański *et al.* 2015, Pan *et al.* 2017, Rao *et al.* 2017, Tang *et al.* 2014, Vu *et al.* 2014, Wan *et al.* 2017, Wang *et al.* 2017, Xiao and Liu 2017a, Xiao *et al.* 2012, Xiao and Liu 2017b, Xiao *et al.* 2018, Xiao *et al.* 2017b, Yang and Yan 2015, Yang and Pan 2015, Zhang *et al.* 2016, Zhang *et al.* 2014, Zhang *et al.* 2018, Zou and Zou 2017, Zou *et al.* 2016, Zou and Xia 2017, Zou *et al.* 2018, Zou and Qian 2018). In recent years, many researchers have investigated the problems of groundwater seepage in tunnel excavation, however, the effect of hydraulic-mechanical coupling still needs to be investigated, especially in strain-softening considering hydraulic-mechanical coupling. For example, the influences of seepage and gravitational loads on elasto-plastic solution of circular tunnels were analyzed by Fahimifar *et al.* (2014). The simplified analytical solutions for the influence of tunnel excavation on the land subsidence were obtained by Lee *et al.* (2007) from an engineering application. However, the theoretical solutions were based on the linear strength criterion and didn't consider the coupling effects of stress and seepage in tunnel excavation. Kolymbas and Wagner (2007) proposed the analytical solutions for groundwater seepage with a dynamic water head in the deep buried tunnel and shallow buried tunnel, respectively. But the solutions obtained can only be applied to solving the problems of groundwater seepage in linear surrounding rock and were not suitable for the case of hydraulic-mechanical coupling. The analytical solutions for steady-state groundwater inflow into a drained circular tunnel in a semi-infinite aquifer were discussed by Kyung *et al.* (2008). Fahimifar *et al.* (2015a) proposed a new solution to calculate pore water pressure, stress, and strain distributions on periphery of circular tunnels in axisymmetric and plain strain conditions compatible with a nonlinear Hoek-Brown yield criterion and a modified non-radial flow pattern for the hydraulic analysis. Fahimifar *et al.* (2015b) proposed an analytical–numerical model for elasto-plastic analysis of underwater tunnels that considers seepage body forces and strain-softening behavior, and a theoretical solution was also presented for calculation of the pore-water pressure, stress and strain distributions around the circular tunnels in axisymmetric and plain strain conditions by using the finite difference method. Fahimifar and Zareifard (2009) developed the coupling analysis for groundwater seepage after tunnel excavation on the basis of the theories of Kolymbas and Wagner (2007), nevertheless, the analytical solutions are not given considering hydraulic-mechanical coupling. Therefore, it is a numerical technique problem for obtaining the solution for stress and displacement of strain-softening surrounding rock, especially considering hydraulic-mechanical coupling.

The main objective of this study was to investigate the properties of stress and displacement in the strain-softening

*Corresponding author, Professor
E-mail: zoujinfeng_csu@163.com

ISSN: 2005-307X (Print), 2092-6219 (Online)

surrounding rock considering hydraulic-mechanical coupling. The innovations of this study can be concluded as follows.

(1) The radius-incremental-approach was reconstructed and a novel approach for calculating stress, displacement and plastic radius for circular tunnel considering hydraulic-mechanical coupling was developed.

(2) The whole plastic zone was divided into a finite number of concentric annuli by radius, and stress and displacement of each annulus were determined in terms of numerical method and Terzaghi's effective stress principle. The proposed technique can be used to assess the reliability of tunnel supporting scheme by convergence constraint method and provide reference for the design of tunnel support.

2. Methodology

2.1 Problem definition

As is shown in Fig. 1, the tunnel with radius r_o is assumed to be excavated in a continuous, homogeneous, isotropic, initially elastic rock mass. The cross-section of the tunnel is subjected to a hydrostatic pressure (σ_0) and a pore water pressure [$p(r,\theta)$]. The internal supporting pressure p_{in} acts uniformly on the tunnel wall surface in radial direction. Axial symmetry condition for geometry and loading is assumed in this study, therefore, stress and displacement of surrounding rock are the functions of radius r. It is also assumed that σ_1 and σ_3 represent the maximum and minimum principal stresses, respectively, σ_r and σ_θ represent the radial and circumferential stresses, respectively. σ_c is the uniaxial compressive strength of the surrounding rock. F_r and $p_w(r,\theta)$ are the seepage force and the pore water pressure acting on the surrounding rock, respectively. R is plastic radius and R_s is softening radius, respectively.

The distributions of seepage force and pore water pressure don't satisfy the axisymmetrical conditions in hydraulic analysis, because the pore water pressure p_w=$p_w(r,\theta)$ is the function of radius r and the direction angle θ. We make θ=0° (i.e., in horizontal direction) in this study to analyze the hydraulic-mechanical coupling, the solutions at other directions can also be calculated by the same method, solutions of stress and displacement can be obtained by linear superposition method.

On the basis of the theories in elastic mechanics and Terzaghi's effective stress principle, the following stress equilibrium equation should be satisfied at any radius of surrounding rock.

$$\frac{d\sigma_r^{'}}{dr}-\frac{\sigma_\theta^{'}-\sigma_r^{'}}{r}+\frac{dp_w}{dr}=0 \tag{1}$$

2.2 Pore water pressure and seepage force

In a pressure tunnel, below groundwater table, the applied seepage body forces are generated by the pore water pressure gradients. The circular tunnel is excavated under

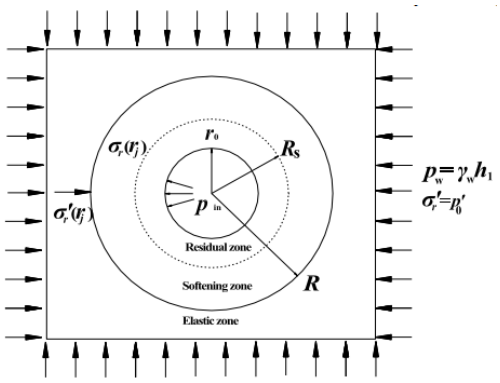

Fig. 1 Axisymmetric model of tunnel excavation

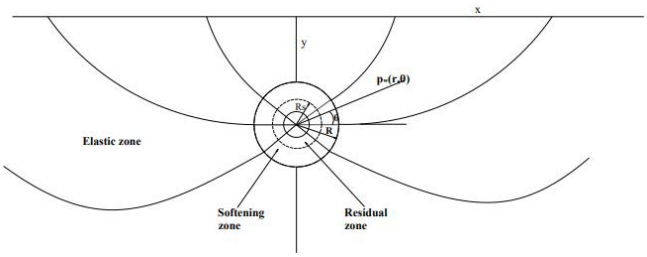

Fig. 2 Model of seepage network

groundwater level and the groundwater surface remains unchanged in this study. The seepage network around the surrounding rock can be presented in Figure 2. The pore water pressure $p_w(r,\theta)$ is the function of radial distance from center of cavity r and the angle measured clockwise from the horizontal direction θ. The hydraulic head is related to the pore water pressure at any point of the surrounding rock and the formula of the pore water pressure can be obtained from Bernoulli equation ($p_w(r,\theta)/\gamma_w+r\sin\theta=h_w(r,\theta)$), where r,θ are all polar coordinates in the plane, γ_w is the specific gravity of water and h_w represents hydraulic head. It is also assumed that the seepage flow is along the radial direction, the water head on the elastic-plastic boundary remains constant and the inward seepage flow rate (q) is positive in the calculation.

Pore water pressure can be derived from Bernoulli equation and presented as follows (Zou and Li 2015).

$$p_w(r,\theta)=\frac{\alpha}{2}\log\left(\frac{c^2r^2\cos^2\theta+\left(c\,r\sin\theta-c^2R\right)^2}{c^2r^2\cos^2\theta+\left(c\,r\sin\theta-R\right)^2}\right), \tag{2}$$

$$c=\frac{h_1-\sqrt{h_1^2-R^2}}{R^2}, \tag{3}$$

$$\alpha=\frac{P_{w(R)}^f-\gamma_w h_1}{\log(c)}, \tag{4}$$

$$p_w(r,\theta=0)=\frac{\alpha}{2}\log\left(\frac{c^2r^2+c^4R^2}{c^2r^2+R^2}\right) \tag{5}$$

where, R is the plastic radius of surrounding rock, h_1 is the distance from the center of the tunnel to the groundwater surface. The equation $P^f_{w(r_0)} = H^f_{w(R)}\gamma_w$ is used to calculate the final pore water pressure at the elastic-plastic boundary, $H^f_{w(R)}$ here represents the final water head at the interface of the elastic and plastic zone, γ_w represents the specific gravity of water.

The relationship between the seepage force along the radial direction and the pore water pressure can be described by

$$F_r = \beta \frac{dp_w(r,\theta)}{dr}, \tag{6}$$

where, β is the Biot-Willis coupling poroelastic constant and is assumed to be 1 in this study (Zou and Li 2015).

2.3 Equation of hydraulic-mechanical coupling

The hydraulic-mechanical coupling equation can be expressed as (Brown and Bray 1982)

$$k_r = k_{0r}\left(1+\eta\varepsilon_v^2\right), \tag{7}$$

where, k_r represents the seepage force coefficient in plastic zone of surrounding rock and it's closely related to the strain of surrounding rock. K_{0r} represents the initial seepage force coefficient of surrounding rock, which is equal to the elastic seepage force coefficient. $\varepsilon_v = \varepsilon_1 + \varepsilon_3$ (or $\varepsilon_v = \varepsilon_\theta + \varepsilon_r$), where, ε_v is volume strain and η is coupling coefficient.

Pore water pressure and seepage discharge q in plastic zone can be illustrated as follows.

$$p_w(r,\theta) = \frac{\gamma_w q}{2\pi}\int_{r_0}^{r}\frac{1}{k_r(r)}dr + p_w(r_0,\theta) \tag{8}$$

$$q = \frac{2\pi\left(\gamma_w h_1 - p_w(r_0,\theta)\right)}{\int_{r_0}^{r}\frac{\gamma_w}{k_r(r)}dr - \frac{\gamma_w}{k_{0r}}\log(c)} \tag{9}$$

2.4 Yield criterion

Yield criterions adopted in this study are Hoek-Brown (H-B) yield criterion (including generalized H-B yield criterion) and Mohr-Coulomb (M-C) yield criterion. Generalized H-B yield criterion is expressed as follows.

$$\sigma_1 = \sigma_3 + \sigma_c\left(m\frac{\sigma_3}{\sigma_c} + s\right)^a \tag{10}$$

where, σ_c is uniaxial compressive strength of surrounding rock. σ_1 and σ_3 are the maximum and minimum principal stresses, respectively. m, s, a are all the strength parameters. When a_r=a_p=0.5, the generalized H-B yield criterion will become H-B yield criterion.

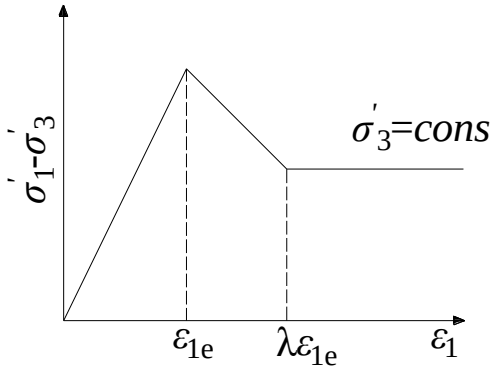

Fig. 3 Relationship of stress and strain in the strain-softening surrounding rock

Mohr-Coulomb (M-C) yield criterion is shown as follows.

$$\sigma_1 = N\sigma_3 + Y \tag{11}$$

where, σ_1 and σ_3 are the maximum and minimum principal stresses, respectively. $N = (1+\sin\varphi)/(1-\sin\varphi)$ and $Y = 2c\cos\varphi/(1-\sin\varphi)$, where, c and φ are the cohesion and friction angle, respectively.

2.5 Strain-softening model

The strain-softening characteristic adopted in this study is shown in Fig. 3.

A softening coefficient γ is employed to control the yield process (or the plastic potential) from a peak one to a residual one and expressed as follows (Alonso *et al.* 2003).

$$\gamma = \varepsilon_1^p - \varepsilon_3^p \tag{12}$$

where, γ^* is the critical softening coefficient. When 0< γ < γ^* and $\gamma \geq \gamma^*$, the residual behavior and the residual zone in surrounding rock will appear. As shown in the Fig. 3. ε_{1e} is the critical value of elastic strain, and λ is a constant.

2.6 Plastic potential function and flow rule

According to the plasticity increment theory, the plastic strain increment can be determined by the plastic potential function and defined by

$$\varepsilon_r^p = -k\varepsilon_\theta^p \tag{13}$$

where, k is the dilation factor and it can be written as

$$k = \frac{1+\sin\psi}{1-\sin\psi} \tag{14}$$

where, ψ is dilation angle. When ψ is equal to the friction angle of the surrounding rock, the associated flow rule can be adopt, or the non-associated flow rule should be adopt. When k=1, there is no plastic volume strain in plastic zone.

2.7 Degradation of strength and deformation parameters

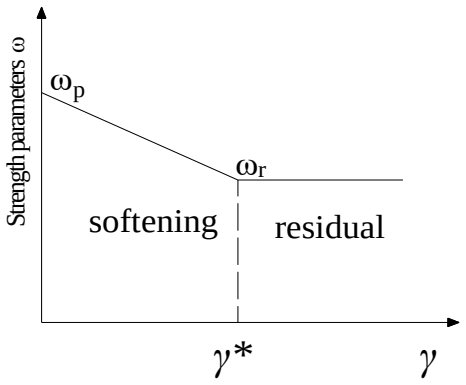

Fig. 4 Linear reduction process of the strength of surrounding rock

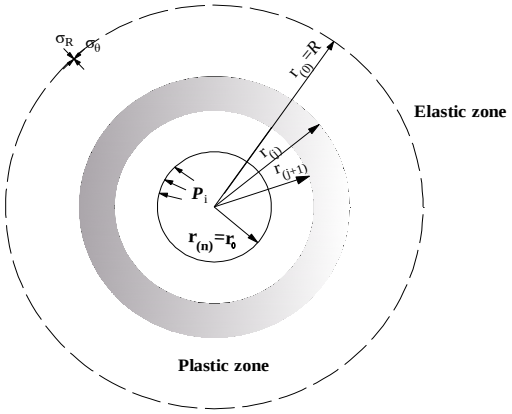

Fig. 5 Calculation model in plastic zone

In terms of the strain-softening model, the strength of surrounding rock doesn't suddenly drop to its residual strength in the yield process, but it is a linear decline process (i.e., the strain-softening process). Linear reduction process of the strength of surrounding rock is adopted in this study and as shown in Fig. 4 (Alonso *et al.*, 2003).

In plastic zone, the strength and deformation parameters of surrounding rock should satisfy with the following linear equation (Alonso *et al.* 2003).

$$\omega\left(\gamma^{\mathrm{p}}\right)=\begin{cases}\omega_{\mathrm{p}}-\left(\omega_{\mathrm{p}}-\omega_{\mathrm{r}}\right)\dfrac{\gamma}{\gamma^{*}}, & 0<\gamma<\gamma^{*}\\ \omega_{\mathrm{r}}, & \gamma\geq\gamma^{*}\end{cases} \tag{15}$$

where, ω represents the strength and deformation parameters of surrounding rock, such as c, φ, m, s, a and ψ. ω_p and ω_r are the peak and residual values, respectively. γ is the softening coefficient (i.e., deviatoric plastic strain), and γ^* is critical value of softening coefficient and the value of γ^* can be obtained by experiment.

3. Solutions

3.1 Stress and displacement in the plastic zone

It's difficult to obtain the analytical solutions for stress and displacement in plastic zone when considering the effects of strain-softening characteristic and hydraulic-mechanical coupling. Therefore, stress and displacement in plastic zone can be calculated by the numerical method. The whole plastic zone in this study is divided into a finite number of concentric annuli, and stress and strain of each annulus can be calculated according to the stress equilibrium equation and the compatibility equation. When stress and strain of one annulus are obtained, the results can be iterated to the next annulus until the stress and strain in plastic zone are all determined. The calculation model is shown in Fig. 5.

As is shown in Fig. 5, the outer radius of the *jth* annulus is $r_{(j)}$ and the inner radius is $r_{(j+1)}$. The thickness of each annulus is Δr. The radius of j+1*th* annulus in plastic zone can be expressed by

$$r_{(j+1)}=r_{(j)}+\Delta r \tag{16}$$

For M-C yield criterion, combining Eqs. (1), (11), (16), the stresses of *jth* annulus can be obtained as follows.

$$\begin{cases}\sigma'_{r(j+1)}=\dfrac{\dfrac{\sigma'_{r(j)}}{r_{(j+1)}-r_{(j)}}+\dfrac{\left(N_{(j)}-1\right)\sigma'_{r(j)}+2Y_{(j)}}{r_{(j+1)}+r_{(j)}}-\dfrac{p_{wr(j+1)}-p_{wr(j)}}{r_{(j+1)}-r_{(j)}}}{\dfrac{1}{r_{(j+1)}-r_{(j)}}-\dfrac{N_{(j)}-1}{r_{(j+1)}+r_{(j)}}}\\ \sigma'_{\theta(j+1)}=N_{(j)}\dfrac{\dfrac{\sigma'_{r(j)}}{r_{(j+1)}-r_{(j)}}+\dfrac{\left(N_{(j)}-1\right)\sigma'_{r(j)}+2Y_{(j)}}{r_{(j+1)}+r_{(j)}}-\dfrac{p_{wr(j+1)}-p_{wr(j)}}{r_{(j+1)}-r_{(j)}}}{\dfrac{1}{r_{(j+1)}-r_{(j)}}-\dfrac{N_{(j)}-1}{r_{(j+1)}+r_{(j)}}}+Y_{(j)}\end{cases} \tag{17}$$

For H-B yield criterion, combining Eqs. (1), (10), (16), the stress of *jth* annulus can be obtained as follows.

$$\begin{cases}\sigma'_{r(j+1)}=A_r^2m_{(j)}\sigma_{c(j)}-\Delta p_w+\sigma'_{r(j)}+A_r\sqrt{\sigma_{c(j)}\left[\left(A_r^2m_{(j)}^2+4s_{(j)}\right)\sigma_{c(j)}+\left(-2\Delta p_w+4\sigma'_{r(j)}\right)m_{(j)}\right]}\\ \sigma'_{\theta(j+1)}=A_r^2m_{(j)}\sigma_{c(j)}-\Delta p_w+\sigma'_{r(j)}+A_r\sqrt{\sigma_{c(j)}\left[\left(A_r^2m_{(j)}^2+4s_{(j)}\right)\sigma_{c(j)}+\left(-2\Delta p_w+4\sigma'_{r(j)}\right)m_{(j)}\right]}+\\ \sigma_{c(j)}\left(m_{(j)}\dfrac{A_r^2m_{(j)}\sigma_{c(j)}-\Delta p_w+\sigma'_{r(j)}+A_r\sqrt{\sigma_{c(j)}\left[\left(A_r^2m_{(j)}^2+4s_{(j)}\right)\sigma_{c(j)}+\left(-2\Delta p_w+4\sigma'_{r(j)}\right)m_{(j)}\right]}}{\sigma_{c(j)}}+s_{(j)}\right)^{0.5}\end{cases} \tag{18}$$

where, $A_r=\dfrac{r_{(j+1)}-r_{(j)}}{r_{(j+1)}+r_{(j)}}$ and $\Delta p_w=p_{wr(j+1)}-p_{wr(j)}$.

For generalized H-B yield criterion, the following expression can be determined.

$$\frac{\sigma'_{r(j+1)}-\sigma'_{r(j)}}{r_{(j+1)}-r_{(j)}}-\frac{\left[m_{(j)}\sigma_{c(j)}\left(\sigma'_{r(j+1)}+\sigma'_{r(j)}\right)/2+s_{(j)}\sigma_{c(j)}^2\right]^{a_{(j)}}}{\left(r_{(j+1)}+r_{(j)}\right)/2}+\frac{p_{wr(j+1)}-p_{wr(j)}}{r_{(j+1)}-r_{(j)}}=0 \tag{19}$$

Solving Eq. (19) using the numerical method, $\sigma'_{\theta(j+1)}$ can be obtained by substituting the radial stress of j+1*th* annulus $\sigma'_{r(j+1)}$ into Eq. (10).

When stress of each annulus is obtained, strain can also be calculated by the flow rule and the compatibility equation. According to the finite difference method, the compatibility equation can be illustrated as follows.

$$\frac{d\varepsilon_{\theta(j)}}{dr}+\frac{\varepsilon_{\theta(j+1)}-\varepsilon_{r(j+1)}}{\bar{r}_{(j)}}=0 \tag{20}$$

where, $\bar{r}_{(j)}=\left(r_{(j)}+r_{(j+1)}\right)/2$ and $d\varepsilon_{\theta(j)}=\varepsilon_{\theta(j+1)}-\varepsilon_{\theta(j)}$.

Subsequently, Eq. (20) becomes

$$\frac{d\varepsilon_{\theta(j)}^{p}}{dr}+\frac{\varepsilon_{\theta(j+1)}^{p}-\varepsilon_{r(j+1)}^{p}}{\bar{r}_{(j)}}=-\frac{d\varepsilon_{\theta(j)}^{e}}{dr}-\frac{\varepsilon_{\theta(j+1)}^{e}-\varepsilon_{r(j+1)}^{e}}{\bar{r}_{(j)}} \tag{21}$$

where, ε_r^e and ε_θ^e represent the elastic radial and circumferential strains, respectively, ε_r^p and ε_θ^p represent the plastic radial and circumferential strains, respectively.

Combining Eqs. (13), (16), (21), plastic strains of *jth* annulus can be obtained as follows.

$$\begin{cases} \varepsilon_{\theta(j+1)}^p = \dfrac{-\dfrac{\varepsilon_{\theta(j+1)}^e-\varepsilon_{\theta(j)}^e}{\Delta r}-\dfrac{\overline{\varepsilon_{\theta(j)}^e}-\overline{\varepsilon_{r(j)}^e}}{\overline{r_{(j)}}}+\varepsilon_{\theta(j)}^p\left[\dfrac{1}{\Delta r}-\left(1+k_{(j)}\right)\dfrac{1}{r_{(j+1)}+r_{(j)}}\right]}{\dfrac{1}{\Delta r}+\left(1+k_{(j)}\right)\dfrac{1}{r_{(j+1)}+r_{(j)}}} \\ \varepsilon_{r(j+1)}^p = k\dfrac{\dfrac{\varepsilon_{\theta(j+1)}^e-\varepsilon_{\theta(j)}^e}{\Delta r}+\dfrac{\overline{\varepsilon_{\theta(j)}^e}-\overline{\varepsilon_{r(j)}^e}}{\overline{r_{(j)}}}-\varepsilon_{\theta(j)}^p\left[\dfrac{1}{\Delta r}-\left(1+k_{(j)}\right)\dfrac{1}{r_{(j+1)}+r_{(j)}}\right]}{\dfrac{1}{\Delta r}+\left(1+k_{(j)}\right)\dfrac{1}{r_{(j+1)}+r_{(j)}}} \end{cases} \tag{22}$$

$$\begin{cases} \varepsilon_{r(j+1)}^e = \dfrac{1}{E}\left[\left(\sigma_{r(j+1)}^{'}-p_0\right)-\nu\left(\sigma_{\theta(j+1)}^{'}-p_0\right)\right] \\ \varepsilon_{\theta(j+1)}^e = \dfrac{1}{E}\left[\left(\sigma_{\theta(j+1)}^{'}-p_0\right)-\nu\left(\sigma_{r(j+1)}^{'}-p_0\right)\right] \end{cases} \tag{23}$$

Elastic strains of *j*+1*th* annulus $\varepsilon_{r(j+1)}^e$ and $\varepsilon_{\theta(j+1)}^e$ can be obtained by Hooke's law (Eq. (23)). Therefore, $\varepsilon_{r(j+1)}$ and $\varepsilon_{\theta(j+1)}$ can also be calculated. The results are expressed by

$$\begin{cases} \varepsilon_{\theta(j+1)} = \varepsilon_{\theta(j+1)}^p + \varepsilon_{\theta(j+1)}^e \\ \varepsilon_{r(j+1)} = \varepsilon_{r(j+1)}^p + \varepsilon_{r(j+1)}^e \end{cases} \tag{24}$$

In the light of the relationship between displacement and strain, displacement of *j*+1*th* annulus can be defined as follows.

$$u_{(j+1)} = r_{(j+1)}\varepsilon_{\theta(j+1)} \tag{25}$$

Solutions of stress and displacement in plastic zone can be obtained through several iterations. The detailed calculation procedure can be described as follows.

(1) It is assumed that there is no water pressure in surrounding rock, when a plastic radius R_p is assumed, and then stress and strain are determined in plastic zone.

(2) According to the assumed plastic radius, stress and strain in plastic zone under the effects of hydraulic-mechanical coupling can be determined by Eqs. (20) and (23).

(3) If the absolute value of the difference is larger than [δσ], which is between the stress acting on the wall of tunnel obtained in the first step and the corresponding stress is also obtained in the second step, the iterations in step (2) should be continue until the difference is less than [δσ].

(4) If a series of plastic radius R_p assumed and repeat steps (1), (2), and (3), R_p–p_{in} curve is obtained. The real plastic radius R_p can be obtained by interpolation method in terms of the known value of internal supporting pressure p_{in}.

3.2 Stress and displacement in elastic zone

Relationship of displacement and strain in the elastic zone can be presented by,

$$\begin{cases} \varepsilon_r = -\dfrac{du}{dr} \\ \varepsilon_\theta = -\dfrac{u}{r} \end{cases}, \tag{26}$$

In the light of Hooke's law, the radial and circumferential effective stresses in elastic zone can be expressed as follows

$$\sigma_\theta^{'} = \frac{E}{(1+\nu)(1-2\nu)}\left[(1-\nu)\varepsilon_\theta^e + \nu\varepsilon_r^e\right] \tag{27}$$

$$\sigma_r^{'} = \frac{E}{(1+\nu)(1-2\nu)}\left[(1-\nu)\varepsilon_r^e + \nu\varepsilon_\theta^e\right] \tag{28}$$

Substituting Eqs. (26), (27), (28) into Eq. (1), the following second-order differential equation of displacement can be derived.

$$\frac{d^2u}{dr^2}+\frac{1}{r}\frac{du}{dr}-\frac{u}{r^2} = \frac{dp_w}{dr}\frac{(1+\nu)(1-2\nu)}{E(1-\nu)}, \tag{29}$$

Eq. (29) is a second-order linear differential equation, it can be solved by the superposition method (i.e., the total displacement can be decomposed into the sum of the u^w and u^b, where u^w and u^b are the displacement induced by seepage force and boundary conditions ($\sigma_r(r=R)=\sigma_R$, $\sigma_r=\sigma_0(r\to\infty)$), respectively).

The two parts of total displacement can be calculated by solving the differential Eq. (29) (Fahimifar *et al.* 2015b).

$$u^w(r) = C_1 r + \frac{1}{r}C_2 - \frac{1}{4}\frac{(1+\nu)(1-2\nu)\alpha}{Ec^2r(1-\nu)}\left[\begin{array}{l} c^4R^2\log\left(r^2+c^2R^2\right)+c^2r^2\log\left(\dfrac{r^2+c^2R^2}{R^2+c^2r^2}\right) \\ -R^2\log\left(R^2+c^2r^2\right)\end{array}\right] \tag{30}$$

$$\varepsilon^w{}_{\theta(r)} = C_1 + \frac{1}{r^2}C_2 - \frac{1}{4}\frac{(1+\nu)(1-2\nu)\alpha}{Ec^2r^2(1-\nu)}\left[\begin{array}{l} c^4R^2\log\left(r^2+c^2R^2\right)+c^2r^2\log\left(\dfrac{r^2+c^2R^2}{R^2+c^2r^2}\right) \\ -R^2\log\left(R^2+c^2r^2\right)\end{array}\right] \tag{31}$$

$$\varepsilon^w{}_{r(r)} = C_1 - \frac{1}{r^2}C_2 - \frac{1}{4}\frac{\alpha(1+\nu)(1-2\nu)}{Ec^2r^2(1-\nu)}\left[\begin{array}{l} \dfrac{2c^4R^2r^2}{r^2+c^2R^2}-\dfrac{2c^2R^2r^2}{R^2+c^2r^2}+2c^2r^2\log\left(\dfrac{r^2+c^2R^2}{R^2+c^2r^2}\right) \\ +\dfrac{c^2r^3\left(R^2+c^2r^2\right)\left(\dfrac{2r}{R^2+c^2r^2}-\dfrac{2c^2r\left(c^2R^2+r^2\right)}{\left(R^2+c^2r^2\right)}\right)}{r^2+c^2R^2} \\ +c^4R^2\log\left(r^2+R^2c^2\right)+c^2r^2\log\left(\dfrac{r^2+R^2c^2}{R^2+c^2r^2}\right) \\ -R^2\log\left(R^2+c^2r^2\right)\end{array}\right] \tag{32}$$

where C_1 and C_2 are all the integral constants and can be determined by the boundary conditions (i.e., $\sigma_r(r=R)=\sigma_R$, $\sigma_r=\sigma_0(r\to\infty)$).

$$C_1 = -\frac{1-\nu-2\nu^2}{2E(1-\nu)}\left(P_{w(r_0)} - \gamma_w h_1\right), \tag{33}$$

$$C_2=\frac{\alpha\left(c^4-1\right)R^2\left(2\nu-1\right)\left(1+\nu\right)\log\left(R^2\left(c^2+1\right)\right)}{4Ec_w^2\left(1-\nu\right)}-\frac{\alpha\log\left(c\left(2\nu^2+\nu-1\right)R^2\right)}{2E\left(1-\nu\right)\left(2\nu-1\right)} \quad (34)$$

Substituting the integral constants C_1 and C_2 into Eq. (30), displacement (u^w) induced by seepage force can be obtained.

Substituting the integral constants C_1 and C_2 into Eqs. (31) and (32), the radial and circumferential strains (ε_r^w and ε_θ^w) induced by seepage force can be obtained.

Substituting the integral constants C_1 and C_2 into Eqs. (27) and (28), the radial and circumferential stresses ($\sigma_r^{'w}$ and $\sigma_\theta^{'w}$) induced by seepage force can be obtained.

Displacement and stress induced by the boundary conditions can be given by

$$u^b=-\frac{1+\nu}{E}\left[\left(\sigma_0-\sigma_R\right)\frac{R^2}{r}\right] \quad (35)$$

$$\varepsilon_\theta^b=-\frac{1+\nu}{E}\left[\left(\sigma_0-\sigma_R\right)\frac{R^2}{r^2}\right] \quad (36)$$

$$\varepsilon_r^b=-\frac{1+\nu}{E}\left[\left(\sigma_0-\sigma_R\right)\frac{R^2}{r^2}\right] \quad (37)$$

$$\sigma_r^{'b}=\left(\sigma_R-\sigma_0\right)\frac{R^2}{r^2}+\sigma_0 \quad (38)$$

$$\sigma_\theta^{'b}=-\left(\sigma_R-\sigma_0\right)\frac{R^2}{r^2}+\sigma_0 \quad (39)$$

The total stress and the total displacement can be expressed as follows.

$$u=u^w+u^b \quad (40)$$

$$\sigma_r^{'}=\sigma_r^{'w}+\sigma_r^{'b} \quad (41)$$

$$\sigma_\theta^{'}=\sigma_\theta^{'w}+\sigma_\theta^{'b} \quad (42)$$

4. Verification

In order to validate the reliability of the proposed approach, the GRCs (ground response curve) obtained by the proposed approach are compared with the results in Fahimifar and Zarefard (2009) and Brown and Bray (1982). The parameters in Fahimifar and Zarefard (2009) are adopted and shown as follows: r_0=3, p_0=3 MPa, E=20 GPa, ν=0.25, $\alpha=3.5(\gamma^{p^*}=(\alpha-1)\varepsilon_{\theta 0}^e)$, m_p=0.65, s_p=0.002, m_r=0.2, s_r=0.0001, σ_c=40, k_{0r}=10^{-6} m/s, η=10^5, ψ_p=30°, ψ_r=5.2°. As shown in Fig. 6, the GRCs obtained in this study is basically consistent with the GRCs in Fahimifar and Zarefard (2009). The approach in Brown and Bray (1982) underestimates the results because the stresses in Brown and Bray (1982) are all the total stresses and the seepage force in elastic zone is neglected.

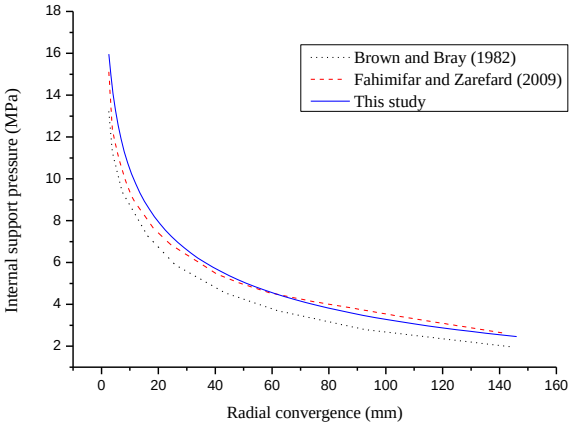

Fig. 6. Comparisons of GRC under H-B yield criterion

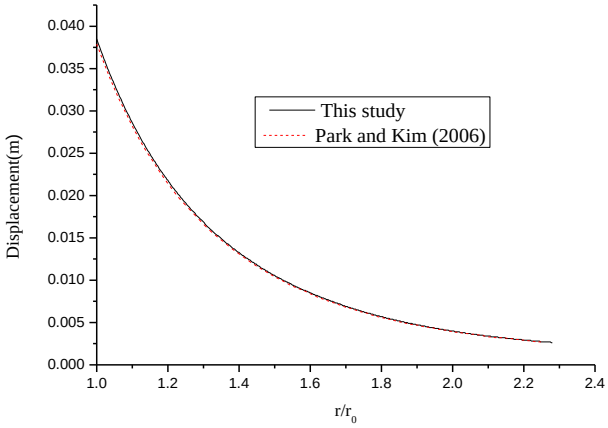

Fig. 7. Displacement under M-C yield criterion

In order to verify the correctness of the proposed approach under M-C yield criterion, the displacement curve obtained in this study is compared with the results in Park and Kim (2006). The parameters in Park and Kim (2006) are adopted as follows: r_0=5 m, p_0=3 MPa, E= 10 GPa, ν= 0.2, c_p=0.5 MPa, c_r=0.2 MPa, φ_p=30°, φ_r=26°, ψ=30°, γ^*=0. As is shown in Fig. 7, the difference between two displacement curves is small. For example, at r=r_0 (i.e., on the wall of the tunnel), displacements are 38.5 mm in this study and 37.9 mm in Park and Kim (2006), respectively, and the difference is (38.5-37.9)/37.9×100%=1.6% . Therefore, the proposed approach is reliable under M-C yield criterion.

5. Application

From a practical point of view, the proposed technique is used for the support design in Yan-zi-dong tunnel. Yan-zi-dong tunnel is located in the expressway from Xupu to Huaihua in Hunan province. GRC can be first obtained by convergence constraint method, therefore, the relationship of the internal support pressure and displacement can be determined. Assuming the support of tunnel is elastic, with the excavation of tunnel, displacement is induced in

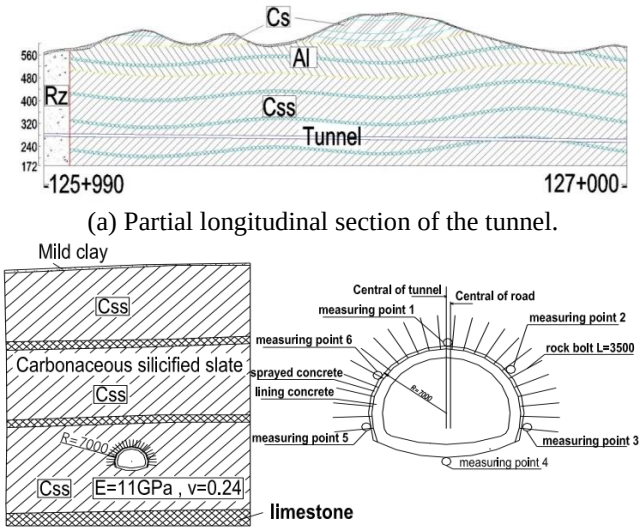

(a) Partial longitudinal section of the tunnel.

(b) Partial cross section of the tunnel

Fig. 8 Partial longitudinal section and the partial cros section of Yan-zi-dong tunnel.

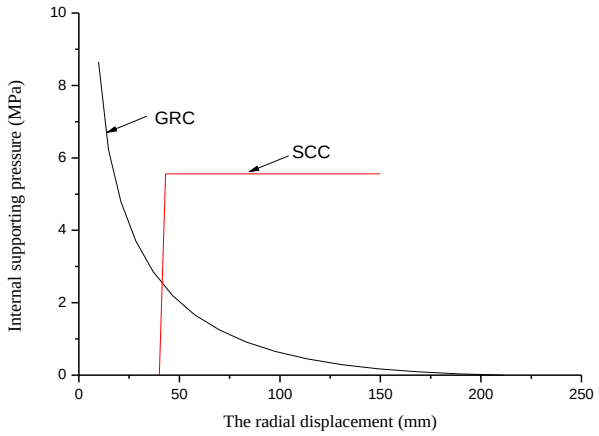

Fig. 9 State of the lining of the tunnel

surrounding rock and the support of tunnel begins to work. The relationship between the tunnel support and the deformation of the surrounding rock can be expressed by SCC (Support Characteristic Curve), the intersection point of two curves (GRC and SCC) indicates the final state of tunnel.

The maximum buried depth of Yan-zi-dong tunnel is about 438.5 m, the length of tunnel is about 4918 m. Class-V surrounding rock here is mainly composed of hard plastic loam, broken strong weathered rock, dissolution fissure and argillaceous strip limestone. The surrounding rock is always broken and is a gravel-like mosaic structure, the self-stability of surrounding rock is always poor. Due to the loose structure of rock mass, it's prone to tunnel collapse when the side wall of Yan-zi-dong tunnel is not supported. The longitudinal and cross sections are shown in Figure 8.

According to the field measurements, the rock or soil mass tests and the monitoring data, the geological and strength parameters of Yan-zi-dong tunnel are collected as follows: r_0=7 m, E=14 GPa, v=0.29, p_0=20 MPa, σ_c=40 MPa, m_p=1.22, m_r=0.36, s_p=0.0021, s_r=0.00008, ψ_p=11°, ψ_r=4°, γ^{p*}=0.004, η=10^5, γ_w=0.001, h_1=400 m, k_{0r}=10^{-6}, a_p=0.51, a_r=0.52. The GRC obtained is shown in Fig. 8. Three-meters long of rock bolt is used in Yan-zi-dong tunnel, 127×76 type double tee iron is adopt to support the tunnel, the thickness of C30 concrete lining can be 1 m and the design safety factor is calculated to be 2.0, Therefore, design of Yan-zi-dong tunnel can accord with the safety requirements.

In fact, the proposed technique can also be used for selecting the optimal supporting scheme for tunnel by obtaining the support characteristic curves corresponding to different tunnel supporting schemes and estimating the final states of the tunnel.

6. Parametric analysis

In order to provide references for engineering design, the effects of coupling coefficient, seepage force, softening coefficient, dilation angle and the strength parameter a on the stress and displacement of tunnel are analyzed under H-B and M-C yield criterion. The important factors that should be selected reasonably in the design of the lining can be determined by the parametric analysis. The other parameters (i.e., except coupling coefficient, seepage force, softening coefficient, dilation angle and the strength parameter a) used for parametric analysis under H-B yield criterion are the same as the parameters in Chapter Four. The parameters used in parametric analysis under M-C yield criterion are given by: r_0=3 m, p_0=20 MPa, E=10 GPa, v=0.25, c_p=1 MPa, c_r=0.7 MPa, φ_p=30°, φ_r=22°, ψ_p=3.75°, ψ_r=3.75°, γ^*=0.008, η=10^5, γ_w=0.001, h_1=300 m, k_{0r}=10^{-6} (from Lee and Pietruszczak (2008)).

6.1 Coupling coefficient

In order to analyze the effects of coupling coefficient on the deformation of surrounding rock, η=0 and η=0.5 are adopt respectively in parametric analysis. The GRC obtained under H-B and M-C yield criteria are shown in Fig. 10(a) and 10(b), respectively.

As is presented in Fig. 10, the differences between two GRC with different coupling coefficients in Figure 10 (a) and (b) are small (about 1.3%), that means the effects of coupling coefficients on the stress and displacement when considering hydraulic-mechanical coupling are small. This conclusion is consistent with the result of Fahimifar and Zarefard (2009).

6.2 Seepage force

In order to analyze the influences of seepage on the deformation of the surrounding rock, the displacement with and without seepage force under H-B or M-C yield criteria are illustrated in Fig. 11(a) and 11(b), respectively. As is shown in Fig. 11, the displacement on the wall of the tunnel without considering seepage force under H-B yield criterion is 39.8 mm and the corresponding displacement obtained with considering seepage force under H-B yield criterion is 52.9 mm, the latter is 32.9% larger than the former. In addition, the effective stress of the surrounding rock will reduce, the plastic radius will increase, when

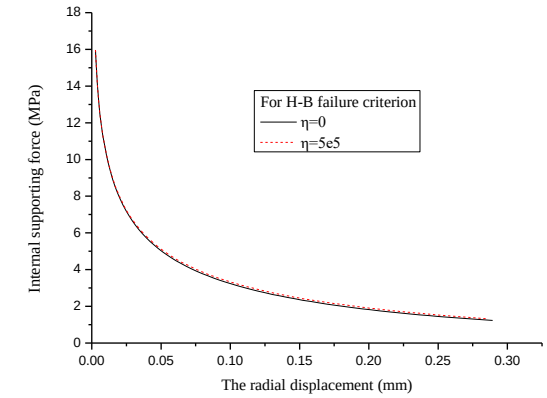

(a) H-B yield criterion

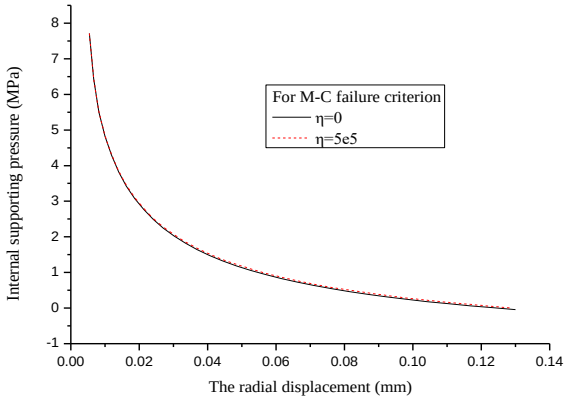

(b) M-C yield criterion

Fig. 10 Comparisons of GRC with different coupling coefficients

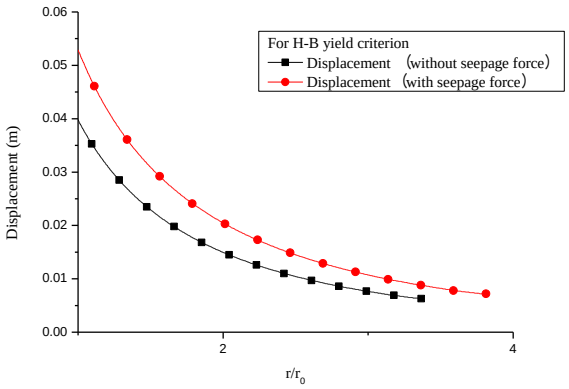

(a) H-B yield criterion

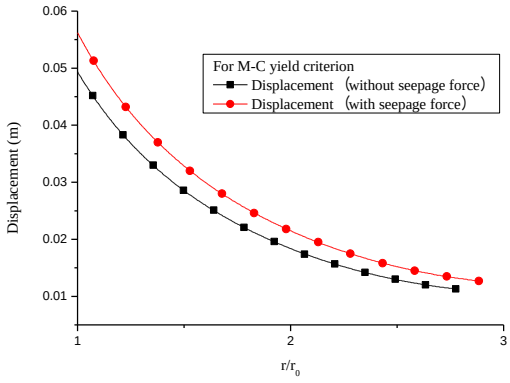

(b) M-C yield criterion

Fig. 11 Comparisons of displacements with and without seepage force

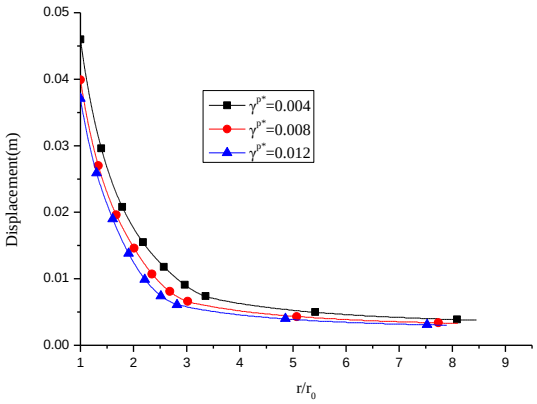

(a) Displacement

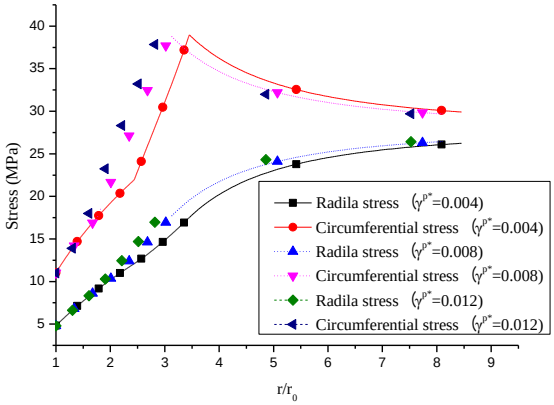

(b) Stress

Fig. 12. Displacement and stress with different softening coefficients under H-B yield criterion

considering the effects of seepage force.

The displacement of the tunnel without considering seepage force and hydraulic-mechanical coupling under M-C yield criterion is 49.4 mm, the corresponding displacement obtained with considering seepage force and hydraulic-mechanical coupling is about 56.2 m, the latter is 13.8% larger than the former. In fact, when considering seepage force and hydraulic-mechanical coupling, the effective stress of surrounding rock will reduce and the plastic radius of surrounding rock will increase. The reason for this is that when considering seepage force and hydraulic-mechanical coupling, the seepage force will reduce the strength parameters of surrounding rock, which results in the increase of plastic radius. Therefore, the effects of seepage force and hydraulic-mechanical coupling on the displacement and stress of surrounding rock are significant and the effects of seepage force on the stress and displacement should be fully considered for the design of the tunnel.

6.3 Softening coefficient

In order to determine the influences of softening coefficients on the stress and displacement of surrounding rock under H-B yield criterion and M-C yield criterion, three cases of critical softening coefficients are adopt in this study. Case 1: γ^*=0.004. Case 2: γ^*=0.008. Case 3: γ^*=0.012. The stress and displacement of surrounding rock

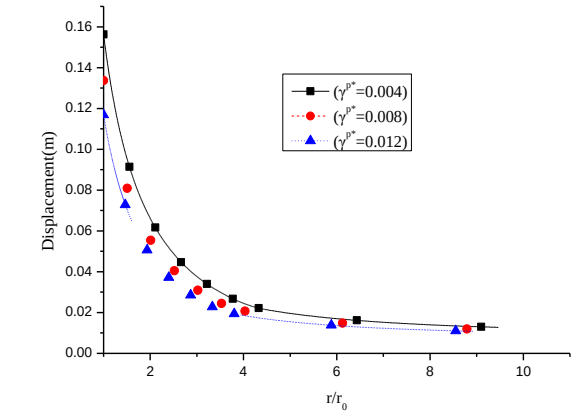

(a) Displacement

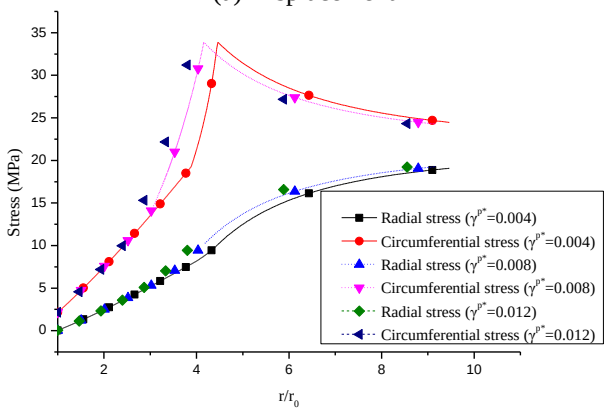

(b) Stress

Fig. 13 Displacement and stress with different softening coefficients under M-C yield criterion

can be calculated by using the methodology in this study. The stress and displacement of surrounding rock with different softening coefficients under H-B yield criterion are presented in Fig. 12, the stress and displacement under M-C yield criterion are described in Fig. 13.

As we can see from Fig. 12, with the gradual increase of the softening coefficient, the displacement and stress of surrounding rock increase, but the plastic radius reduces. The effects of the softening coefficients on the tunnel are nonlinear, i.e., the larger the softening coefficient is, the smaller the influences of softening coefficient on stress and displacement of the surrounding rock are. When the values of γ^* are 0.004, 0.008 and 0.012, the displacements of the tunnel wall are 46.6 mm, 39.9 mm, 37.1 mm, respectively.

The stresses and displacement with different critical softening coefficients under M-C yield criterion are shown in Fig. 13.

As is illustrated in Fig. 13, the influences of critical softening coefficients on the stress and displacement of the surrounding rock under M-C yield criterion are similar to the influence under H-B yield criterion. When the values of γ^* are 0.004, 0.008 and 0.012, the displacements of the tunnel wall are 156.3 mm, 133.7 mm and 116.9 mm, respectively.

6.4 Dilation angle

In order to determine the effect of dilation angle on the deformation of the surrounding rock under H-B yield criterion, three cases of dilation angle under H-B yield criterion are analyzed and displacements can be calculated using the proposed approach. Case 1: ψ_r=ψ_p=30°. Case 2: ψ_p=30°, ψ_r=5.216°. Case 3: ψ_p=ψ_r=5.216°. The results obtained are presented in Fig. 14. At r/r_0=1 (i.e., on the tunnel wall), the displacements in cases 1, 2 and 3 are 0.59 m, 0.055 m and 0.051 m, respectively.

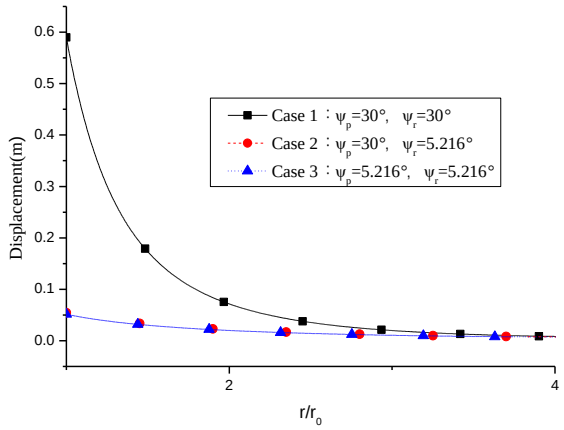

Fig. 14 Displacement of tunnel with different dilation angles under H-B yield criterion

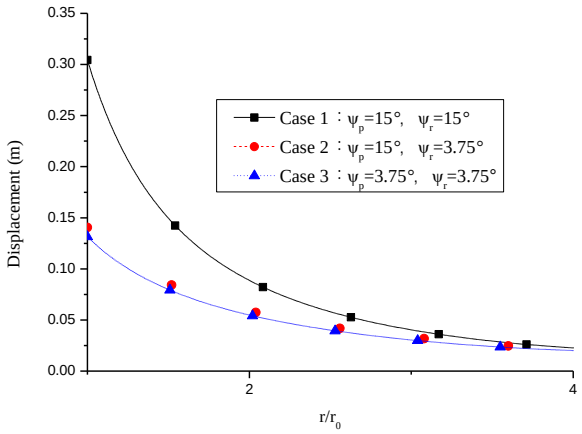

Fig. 15 Displacement of tunnel with different dilation angles under M-C yield criterion

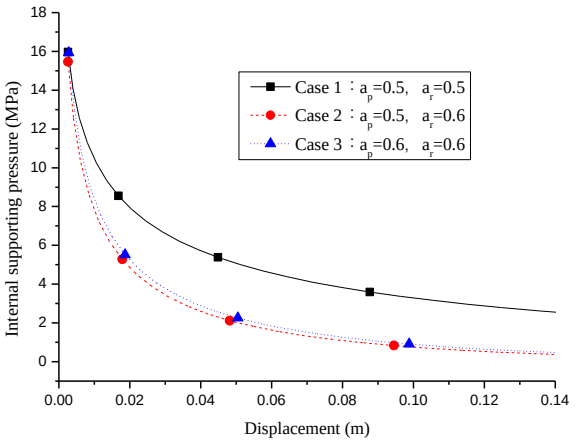

Fig. 16 Influence of different strength parameter *a* on the deformation of the tunnel

In order to study the influence of dilation angle on the deformation of the surrounding rock under M-C yield criterion, three different cases of dilation angles are analyzed and displacement can be calculated using the proposed approach in this study. Case 1: $\psi_r=\psi_p=15°$. Case 2: $\psi_p=15°$, $\psi_r=3.75°$. Case 3: $\psi_r=\psi_p=3.75°$. The displacements obtained are shown in Fig. 15, at $r/r_0=1$ (i.e., on the tunnel wall), the displacements in cases 1, 2 and 3 are 0.3 m, 0.141 m, 0.132 m, respectively.

It can be seen that the peak dilation angle has little influence on the deformation of the surrounding rock, and the influence of residual dilation angle on the deformation of surrounding rock is larger. Moreover, the larger the dilation angle is, the larger the displacement of tunnel surrounding rock is.

6.5 Strength parameter a

In order to study the influence of the strength parameter a on the deformation of the tunnel under H-B yield criterion, three cases of strength parameter a are adopt. That is, case 1: $a_p=a_r=0.5$. Case 2: $a_p=0.5$, $a_r=0.6$. Case 3: $a_p=a_r=0.6$. The results obtained are presented in Fig. 16.

When the displacement of the surrounding rock is 0.135 m, the support forces in cases 1, 2 and 3 are 2.62 MPa, 0.41 MPa and 0.51 MPa, respectively. It can be learned that the influence of a_p on the deformation of the tunnel under H-B yield criterion is small, but the influence of a_r is large enough and the smaller a_r is, the larger the deformation of tunnel is.

7. Conclusions

The properties for stress and displacement of the strain-softening surrounding rock considering the effects of hydraulic-mechanical coupling were investigated. The effects of different strength parameters, seepage force and dilation angle on the results were also studied. Specific conclusions in this note are summarized as follows.

(1) The radius-incremental-approach was reconstructed considering hydraulic-mechanical coupling and strain-softening characteristic.

(2) On the basis of Mohr-Coulomb and Hoek-Brown yield criteria, a novel approach to calculate the stress and displacement of strain-softening surrounding rock was developed in terms of numerical method and Terzaghi's effective stress principle. The proposed approach was demonstrated to be correct by comparing with the results in published literatures.

(3) Combining the actual engineering conditions, the proposed technique is used to assess the reliability of the tunnel support of Yan-zi-dong tunnel by convergence constraint method. In fact, the proposed technique can also be applied to selecting the optimal supporting scheme for tunnel by obtaining the support characteristic curves and estimating the final states of the tunnel corresponding to different tunnel supporting schemes.

Acknowledgements

The authors are grateful to the National Key R&D Program of China (2017YFB1201204).

References

Alonso, E., Alejano, L.R., Varas, F., Fdez-Manín, G. and Carranza-Torres, C. (2003), "Ground response curves for rock masses exhibiting strain-softening behaviour", *J. Numer. Anal. Meth. Geomech.*, **27**(13), 1153-1185.

Antonio, B. (2016), "Deep tunnel in transversely anisotropic rock with groundwater flow", *Rock Mech. Rock Eng.*, **49**(12), 4817-4832.

Apostolos, V. (2017), "A finite strain solution for the elastoplastic ground response curve in tunnelling: Rocks with non-linear failure envelopes", *J. Numer. Anal. Meth. Geomech.*, **41**(3), 1077-1090.

Boonchai, U., Kongkit, Y. and Suraparb, K. (2017), "Three-dimensional undrained tunnel face stability in clay with a linearly increasing shear strength with depth", *Comput. Geotech.*, **88**(8), 146-151.

Brown, E.T. and Bray, J.W. (1982), "Rock-support interaction calculations for pressure shafts and tunnels", *Proceedings of the International Symposium of the International Society for Rock Mechanics*, Aachen, Germany.

Carranza-Torres, C. and Fairhurst, C. (2000), "Application of the convergence-confinement method of tunnel design to rock masses that satisfy the Hoek-Brown failure criterion", *Tunn. Undergr. Sp. Technol.*, **15**(2), 187-213.

Do, N.A., Dias, D., Oreste, P. and Djeran-Maigre, I. (2014), "Three-dimensional numerical simulation for mechanized tunnelling in soft ground: The influence of the joint pattern", *Acta Geotechnica*, **9**(4), 673-694.

El-Tani, M. (2003), "Circular tunnel in a semi-infinite aquifer", *Tunn. Undergr. Sp. Technol.*, **18**(1), 49-55.

Fahimifar, A. and Zareifard, M.R. (2009), "A theoretical solution for analysis of tunnels below groundwater considering the hydraulic-mechanical coupling", *Tunn. Undergr. Sp. Technol.*, **24**(6), 634-646.

Fahimifar, A. and Zareifard, M.R. (2013), "A new closed-form solution for analysis of unlined pressure tunnels under seepage forces", *J. Numer. Anal. Meth. Geomech.*, **37**(11), 1591-1613.

Fahimifar, A. and Zareifard, M.R. (2014), "A new elasto-plastic solution for analysis of underwater tunnels considering strain-dependent permeability", *Struct. Infrastruct. Eng.*, **10**(11), 1432-1450.

Fahimifar, A., Ghadami, H. and Ahmadvand, M. (2014), "The influence of seepage and gravitational loads on elastoplastic solution of circular tunnels", *Scientia Iranica*, **21**(6), 1821-1832.

Fahimifar, A., Ghadami, H. and Ahmadvand, M. (2015a), "An elasto-plastic model for underwater tunnels considering seepage body forces and strain-softening behavior", *Eur. J. Environ. Civ. Eng.*, **19**(2), 129-151.

Fahimifar, A., Ghadami, H. and Ahmadvand, M. (2015b), "The ground response curve of underwater tunnels, excavated in a strain-softening rock mass", *Geomech. Eng.*, **8**(3), 323-359.

Huang, F., Zhao, L.H., Ling, T.H. and Yang, X.L. (2017), "Rock mass collapse mechanism of concealed karst cave beneath deep tunnel", *J. Rock Mech. Min. Sci.*, **91**(1), 133-138.

Ieronymaki, E.S., Whittle, A.J. and Sureda, D.S. (2017), "Interpretation of free-field ground movements caused by mechanized tunnel construction", *J. Geotech. Geoenviron. Eng.*, **143**(4), 04016114.

Kolymbas, D. and Wagner, P. (2007), "Groundwater ingress to tunnels-the exact analytical solution", *Tunn. Undergr. Sp. Technol.*, **22**(1), 23-27.

Kyung, H.P., Adisorn, O. and Lee, J.G. (2008), "Analytical

solution for steady-state groundwater inflow into a drained circular tunnel in a semi-infinite aquifer: A revisit", *Tunn. Undergr. Sp. Technol.*, **23**(2), 206-209.

Lee, S.W., Jung, J.W., Nam, S.W. and Lee, I.M. (2007), "The influence of seepage forces on ground reaction curve of circular opening", *Tunn. Undergr. Sp. Technol.*, **22**(1), 28-38.

Lee, Y.K. and Pietruszczak, S. (2008), "A new numerical procedure for elasto-plastic analysis of a circular opening excavated in a strain-softening rock mass", *Tunn. Undergr. Sp. Technol.*, **23**(5), 588-599.

Liu, C., Zhang, Z.X., Kwok, C.Y., Jiang, H.Q. and Teng, L. (2017), "Ground responses to tunneling in soft soil using the URUP method", *J. Geotech. Geoenviron. Eng.*, **143**(7), 04017023.

Ochmański, M., Modoni, G. and Bzówka, J. (2015), "Numerical analysis of tunneling with jet-grouted canopy", *Soil. Found.*, **55**(5), 929-942.

Pan, Q.J., Xu, J.S. and Dias, D. (2017), "Three-dimensional stability of a slope subjected to seepage forces", *J. Geomech.*, **17**(8), 04017035.

Park, K.H. and Kim, Y.J. (2006), "Analytical solution for a circular opening in an elastic-brittle-plastic rock", *J. Rock Mech. Min. Sci.*, **43**(4), 616-622.

Rao, P.P., Chen, Q.S., Li, L., Nimbalkar, S. and Cui, J.F. (2017), "Elastoplastic solution for spherical cavity expansion in modified cam-clay soil under drained condition", *J. Geomech.*, **17**(8), 06017005.

Tang, X.W., Liu, W., Albers, B. and Savidis, S. (2014), "Upper bound analysis of tunnel face stability in layered soils", *Acta Geotechnica*, **9**(4), 661-671.

Vu, M.N., Broere, W. and Bosch, J.W. (2017), "Structural analysis for shallow tunnels in soft soils", *J. Geomech.*, **17**(8), 04017038.

Wan, M.S.P., Standing, J.R., Potts, D.M. and Burland, J.B. (2017), "Measured short-term ground surface response to EPBM tunnelling in London Clay", *Géotechnique*, **67**(5), 420-445.

Wang, H.N., Zeng, G.S., Utilic, S., Jiang, M.J. and Wu, L. (2017), "Analytical solutions of stresses and displacements for deeply buried twin tunnels in viscoelastic rock", *J. Rock Mech. Min. Sci.*, **93**(3), 13-29.

Xiao, Y. and Liu, G.B. (2017a), "Performance of a large-scale metro interchange station excavation in Shanghai soft clay", *J. Geotech. Geoenviron. Eng.*, **143**(6), 05017003.

Xiao, Y. and Liu, H. (2017), "Elastoplastic constitutive model for rockfill materials considering particle breakage", *J. Geomech.*, **17**(1), 04016041.

Xiao, Y., Liu, H.L., Zhu, J.G. and Shi, W.C. (2012), "Modeling and behaviours of rockfill materials in three-dimensional stress space", *Sci. Chin. Technol. Sci.*, **55**(10), 2877-2892.

Xiao, Y., Stuedlein, A.M., Chen, Q., Liu, H. and Liu, P. (2018), "Stress-strain-strength response and ductility of gravels improved by polyurethane foam adhesive", *J. Geotech. Geoenviron. Eng.*, **144**(2), 04017108.

Xiao, Y., Sun, Y., Yin, F., Liu, H. and Xiang, J. (2017b), "Constitutive modeling for transparent granular soils", *J. Geomech.*, **17**(7), 04016150.

Yang, X.L. and Pan, Q.J. (2015), "Three dimensional seismic and static stability of rock slopes", *Geomech. Eng.*, **8**(1), 97-111.

Yang, X.L. and Yan, R.M. (2015), "Collapse mechanism for deep tunnel subjected to seepage force in layered soils", *Geomech. Eng.*, **8**(5), 741-756.

Zhang, D.M., Huang, H.W., Phoon, K.K. and Hu, Q. F. (2014), "A modified solution of radial subgrade modulus for a circular tunnel in elastic ground", *Soil. Found.*, **54**(2), 225-232.

Zhang, J., Yang, F., Yang, J.S., Zheng, X.C. and Zeng, F.X. (2016), "Upper-bound stability analysis of dual unlined elliptical tunnels in cohesive-frictional soils", *Comput. Geotech.*, **80**(12), 283-289.

Zhang, Q., Zhang, C.H., Jiang, B.S., Li, N. and Wang, Y.C. (2018). "Elastoplastic coupling solution of circular openings in strain-softening rock mass considering pressure-dependent effect", *J. Geomech.*, **18**(1), 04017132.

Zou, J.F. and Qian, Z.H. (2018), "Stability analysis of tunnel face below groundwater considering the coupled flow-deformation", *J. Geomech.*, **18**(8), 04018089.

Zou, J.F. and Xia, M.Y. (2017), "A new approach for the cylindrical cavity expansion problem incorporating deformation dependent of intermediate principal stress", *Geomech. Eng.*, **12**(3), 347-360.

Zou, J.F. and Zou, S.Q. (2017), "Similarity solution for the synchronous grouting of shield tunnels under the non-axisymmetric displacement boundary on vertical surface", *Adv. Appl. Math. Mech.*, **9**(1), 205-232.

Zou, J.F., Chen, K.F. and Pan, Q.J. (2018), "An improved numerical approach of displacement and stress in strain-softening surrounding rock incorporating rockbolt effectiveness and seepage force", *Acta Geotechnica*, 1-21.

Zou, J.F., Xia, Z.Q. and Dan, H.C. (2016), "Theoretical solutions for displacement and stress of a circular opening reinforced by grouted rockbolt", *Geomech. Eng.*, **11**(3), 439-455.

CC